Multiplet-specific shape resonant features in $3\sigma_g$ photoionization of O_2

M. Braunstein and V. McKoy
A. A. Noyes Laboratory of Chemical Physics, California Institute of Technology, Pasadena, California 91125

Maile E. Smith
Institute for Defense Analysis, Alexandria, Virginia 22311

(Received 5 December 1988; accepted 21 December 1988)

We report multiplet-specific photoionization cross sections and photoelectron angular distributions for the $3\sigma_g$ orbital of O_2 leading to the $b\,^4\Sigma_g^-$ and $B\,^2\Sigma_g^-$ ion states obtained using Hartree–Fock photoelectron orbitals. These cross sections show significant nonstatistical behavior at low photoelectron energies which arises from the sensitivity of the $k\sigma_u$ shape resonance to the exchange potentials of these two molecular ions. Specifically, the oscillator strength associated with the shape resonance in the $B\,^2\Sigma_g^-$ cross section is shifted to lower energy compared to that of the $b\,^4\Sigma_g^-$ cross section. This shift gives rise to a quartet to doublet cross section ratio of more than 15:1 near threshold. These effects are difficult to assess in the measured cross sections due to the presence of strong autoionization features. Significant multiplet dependence is also seen in the calculated photoelectron angular distributions.

INTRODUCTION

Recent (2 + 1) resonant-enhanced multiphoton ionization (REMPI) studies via the $C\,^3\Pi_g(3s\sigma_g 1\pi_g)$ and $d\,^1\Pi_g(3s\sigma_g 1\pi_g)$ states of O_2 have shown significant differences in the photoelectron spectra for these two multiplets.[1,2] Strong multiplet-specific effects have also been observed in the 5σ photoionization of NO, where a difference of as much as 3 eV is seen in the positions of the shape resonance in the cross sections for the $A\,^1\Pi(5\sigma^{-1})$ and $b\,^3\Pi(5\sigma^{-1})$ ions.[3,4] These effects arise from differences in the exchange potentials experienced by the photoelectron associated with these multiplets. Such differences can be especially important in shape resonant regions due to the localized nature of the photoelectron wave function. With further development and application of REMPI techniques coupled with high resolution photoelectron spectroscopy,[5] such effects will become increasingly important in our understanding of molecular photoionization dynamics.

Studies of $3\sigma_g$ photoionization of O_2 by Winstead *et al.*[6] using an L^2 Feshbach–Fano formulation of Stieltjes moment theory and multiplet-specific potentials have shown significant nonstatistical behavior in the $b\,^4\Sigma_g^-$ and $B\,^2\Sigma_g^-$ cross sections at energies around the well known $k\sigma_u$ shape resonance.[7–13] Due to strong autoionizing features,[14] these differences are difficult to assess in the experimental photoelectron spectrum. However, recent high-resolution studies[14,15] clearly show multiplet-specific differences in these $3\sigma_g$ cross sections. To further examine these multiplet-specific effects, we have studied the photoionization cross sections and photoelectron angular distributions for the $3\sigma_g$ level of O_2 using Hartree–Fock photoelectron orbitals obtained with the iterative Schwinger method.[16] Our results for these cross sections agree well with those of Winstead *et al.*[6] and, furthermore, show large differences in the multiplet-specific photoelectron angular distributions.

An outline of the paper is as follows. In the next section we discuss the static-exchange potentials used in these multiplet-specific calculations and give a brief description of our method for obtaining the photoelectron orbitals. In the remaining sections we present the results of our studies of the $3\sigma_g$ level of O_2 along with a comparison of these results with experimental data.

THEORY

Multiplet-specific wave functions and potentials

Photoionization of the $3\sigma_g$ orbital of O_2 leads to the $b\,^4\Sigma_g^-$ and $B\,^2\Sigma_g^-$ ion states with experimental ionization potentials 18.17 and 20.29 eV respectively. The dipole-allowed final-state wave functions for photoionization leading to the $b\,^4\Sigma_g^-$ ion are

$$\Psi(^3\Sigma_u^-) = \frac{1}{\sqrt{12}}\big[\,3|(\text{core})3\sigma_g\,\overline{k\sigma_u}\,1\pi_g^+\,1\pi_g^-| - |(\text{core})\,\overline{3\sigma_g}\,k\sigma_u\,1\pi_g^+\,1\pi_g^-| - |(\text{core})3\sigma_g k\sigma_u\,\overline{1\pi_g^+}\,1\pi_g^-| - |(\text{core})3\sigma_g k\sigma_u\,1\pi_g^+\,\overline{1\pi_g^-}|\,\big], \tag{1a}$$

$$\Psi(^3\Pi_u) = \frac{1}{\sqrt{12}}\big[\,3|(\text{core})3\sigma_g\,\overline{k\pi_u^+}\,1\pi_g^+\,1\pi_g^-| - |(\text{core})\,\overline{3\sigma_g}\,k\pi_u^+\,1\pi_g^+\,1\pi_g^-| - |(\text{core})3\sigma_g k\pi_u^+\,\overline{1\pi_g^+}\,1\pi_g^-| - |(\text{core})3\sigma_g k\pi_u^+\,1\pi_g^+\,\overline{1\pi_g^-}|\,\big], \tag{1b}$$

where $(\text{core}) = 1\sigma_g^2 1\sigma_u^2 2\sigma_g^2 2\sigma_u^2 1\pi_u^4$. For photoionization leading to the $B\,^2\Sigma_g^-$ ion, the dipole-allowed final-state wave functions are

 0021-9606/89/083931-06$02.10

$$\Psi(^3\Sigma_u^-) = \frac{1}{\sqrt{6}}\left[2|(\text{core})\ \overline{3\sigma_g} k\sigma_u 1\pi_g^+ 1\pi_g^-| - |(\text{core})3\sigma_g k\sigma_u\ \overline{1\pi_g^+} 1\pi_g^-| \right.$$
$$\left. - |(\text{core})3\sigma_g k\sigma_u 1\pi_g^+\ \overline{1\pi_g^-}|\right], \tag{2a}$$

$$\Psi(^3\Pi_u) = \frac{1}{\sqrt{6}}\left[2|(\text{core})\ \overline{3\sigma_g} k\pi_u^+ 1\pi_g^+ 1\pi_g^-| - |(\text{core})3\sigma_g k\pi_u^+\ \overline{1\pi_g^+} 1\pi_g^-| \right.$$
$$\left. - |(\text{core})3\sigma_g k\pi_u^+ 1\pi_g^+\ \overline{1\pi_g^-}|\right]. \tag{2b}$$

With these wave functions, the static-exchange one-electron equations for the photoelectron orbital ϕ_k can be obtained from the variational expression, $\langle\delta\Psi|H-E|\Psi\rangle = 0$, where H is the fixed-nuclei Hamiltonian and E is the total energy. They are of the form

$$P\left[f + \sum_{\text{core}}(2J_i - K_i) + \sum_{\text{open}}(a_n J_n + b_n K_n) - \epsilon\right]P|\phi_k\rangle = 0, \tag{3}$$

where J_i and K_i are the Coulomb and exchange operators, respectively, P is a projection operator which enforces orthogonality of the continuum orbital to the occupied orbitals,[17] the one-electron operator f is given by

$$f = -1/2\nabla_i^2 - \sum_\alpha \frac{Z_\alpha}{r_{i\alpha}}, \tag{4}$$

Z_α is the nuclear charge, and ϵ is the photoelectron kinetic energy. The coefficients a_n and b_n of Eq. (3) determined using the multiplet-specific wave functions of Eqs. (1) and (2) are given in Table I.

Calculations

The photoelectron orbitals of the static-exchange equations of Eq. (3) were obtained using the iterative Schwinger variational method, discussed extensively elsewhere.[16,17] To solve the Lippmann–Schwinger equations for the continuum orbital associated with the nonlocal molecular ion potential of Eq. (3), the scattering potential is approximated by a separable form,

$$U(\mathbf{r},\mathbf{r}') \cong U^S(\mathbf{r},\mathbf{r}') = \sum_{ij}\langle\mathbf{r}|U|\alpha_i\rangle(U^{-1})_{ij}\langle\alpha_j|U|\mathbf{r}'\rangle, \tag{5}$$

where the matrix U^{-1} is the inverse of the matrix with elements $U_{ij} = \langle\alpha_i|U|\alpha_j\rangle$ and the α_i's are discrete basis functions (see Table II). To ensure convergence of the photoionization cross sections, we use photoelectron orbitals obtained after one step in our iterative procedure.[16,17]

For the ground state of O_2, we used the [3*s*2*p*1*d*] Cartesian Gaussian basis set of Dunning *et al.*[18] Calculations with this basis at the equilibrium geometry of $R(0-0) = 2.282$ a.u. give an SCF energy of $-149.635\ 14$ a.u.

TABLE I. Coefficients of the static-exchange potentials of Eq. (3).

Ion	Channel[a]	a_n/b_n $3\sigma_g$	$1\pi_g^+$	$1\pi_g^-$
$b\,^4\Sigma_g^-$	$^3\Sigma_u^-(k\sigma_u)$	$1/\frac{1}{3}$	$1/\frac{1}{3}$	$1/\frac{1}{3}$
	$^2\Pi_u(k\pi_u)$	$1/\frac{1}{3}$	$1/\frac{1}{3}$	$1/\frac{1}{3}$
$B\,^2\Sigma_g^-$	$^3\Sigma_u^-(k\sigma_u)$	$1/-\frac{1}{3}$	$1/-\frac{5}{6}$	$1/-\frac{5}{6}$
	$^3\Pi_u(k\pi_u)$	$1/-\frac{1}{3}$	$1/-\frac{5}{6}$	$1/-\frac{5}{6}$

[a] Channel symmetry designation of the ion plus photoelectron system.

All matrix elements and functions arising in the solution of the Lippmann–Schwinger equations associated with Eq. (3) were evaluated via single-center expansions about the molecular center. The partial wave expansion of the photoelectron orbital, i.e.,

$$\phi_k^{(-)} = \left(\frac{2}{\pi}\right)^{1/2}\sum_{l=0}^{l_p}\sum_{m=-l}^{+l} i^l\phi_{klm}^{(-)}(\mathbf{r})\,Y_{lm}^*(\Omega_{\hat{k}}), \tag{6}$$

was truncated at $l_p = 7$. The other partial wave expansion parameters were chosen as follows[17]:

(i) maximum partial wave in the expansion of the occupied orbitals in the direct potential = 30,

(ii) maximum partial wave in the expansion of the occupied orbitals in the exchange potential $= 20(1\sigma_g)$, $20(1\sigma_u)$, $10(2\sigma_g)$, $10(2\sigma_u)$, $10(3\sigma_g)$, $10(1\pi_u)$, $10(1\pi_g)$,

TABLE II. Scattering basis sets used in Eq. (5).

Continuum symmetry	Type of Gaussian function[a]	Exponents
σ_u	Cartesian s	16.0,8.0,4.0,2.0,1.0,0.5
	z	1.0,0.5
	Spherical $l=1$	4.0,2.0,1.0,0.5
	$l=3$	4.0,2.0,1.0,0.5
	$l=5$	1.0,0.5
π_u	Cartesian x	8.0,4.0,2.0,1.0,0.5
	Spherical xz	0.5
	$l=1$	1.0
	$l=3$	1.0

[a] Cartesian functions are centered at the nuclei and the spherical functions at the molecular center. For details of the forms of these functions and their use see Ref. 17.

(iii) maximum partial wave in the expansion of $1/r_{12}$ in the direct and exchange terms $= 60$ and 30, respectively,

(iv) all other partial wave expansions were truncated at $l = 30$.

Based on earlier convergence studies,[17] this choice of expansion parameters should provide photoionization cross sections within a few percent of the converged values. The associated radial integrals were obtained with a Simpson's rule quadrature. The grid contained 800 points and extended out to 64.0 a.u. with a step size of 0.01 a.u. from the origin to 2.0 a.u. Beyond 2.0 a.u. the largest step size was 0.16 a.u.

RESULTS AND DISCUSSION

Figure 1 shows the calculated eigenphase sums for the $k\sigma_u$ continuum for the two ion cores. These multiplet-specific eigenphase sums are quite different. The $b\,^4\Sigma_g^-$ eigenphase sum illustrates shape resonance behavior with a rapid increase starting at threshold. The $B\,^2\Sigma_g^-$ eigenphase sum also shows shape resonant behavior, but this behavior suggests that the discrete oscillator strength distribution below this threshold must be perturbed. Studies by Morin *et al.*[14] show significant Rydberg–valence mixing for the low members of the $np\sigma_u$ series leading to the $B\,^2\Sigma_g^-$ ion. To examine this effect on the discrete spectrum we have calculated the oscillator strengths for the first four members of this Rydberg series. The oscillator strength f_n is given by

$$f_n = 4/9E\,|\langle\phi(3\sigma_g)|z|n\sigma_u\rangle|^2. \quad (7)$$

The factor of 4/9 is due to the multiplicity of the final state ion and E is the excitation energy in a.u. The $np\sigma_u$ orbitals were obtained using the improved virtual orbital (IVO) approximation[19] with our SCF basis augmented by a set of p functions with exponents of 0.1, 0.05, 0.025, 0.001 25, and 0.000 625 at the molecular center. Figure 2 shows the resulting oscillator strength in histogram form for the $n\sigma_u$ Rydberg series of the $B\,^2\Sigma_g^-$ ion and the adjoining $k\sigma_u$ continuum cross section. The height and width of each step in the histogram are $f_n\,(dn/dE)$ and dE/dn, respectively.[20] These results show that the σ_u spectral distribution for the $B\,^2\Sigma_g^-$ state is strongly perturbed below threshold. Our calculated discrete spectrum agrees qualitatively with the results of Winstead *et al.*[6] obtained with a more extensive basis set.

In Fig. 3 we show our calculated $3\sigma_g$ photoionization cross sections along with those of Winstead *et al.*[6] leading to the $b\,^4\Sigma_g^-$ (IP = 18.17 eV) and $B\,^2\Sigma_g^-$ (IP = 20.29 eV) ions. The behavior near threshold in the cross sections for

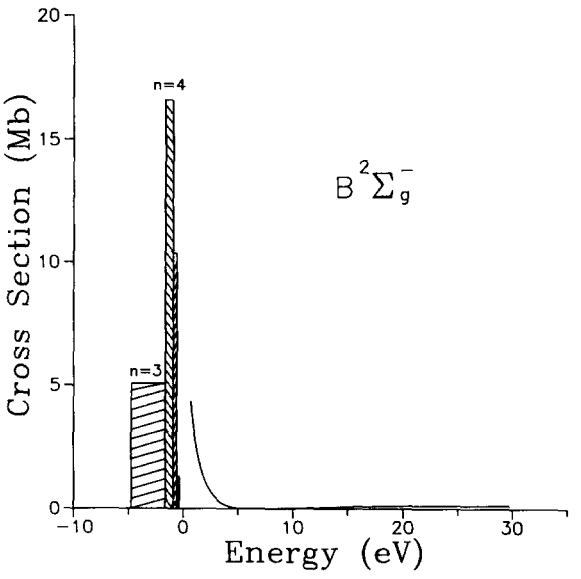

FIG. 2. Oscillator strength distribution in the discrete and continuous spectra for the $3\sigma_g \rightarrow \sigma_u$ transition. The energy scale is relative to the ionization threshold of 20.29 eV.

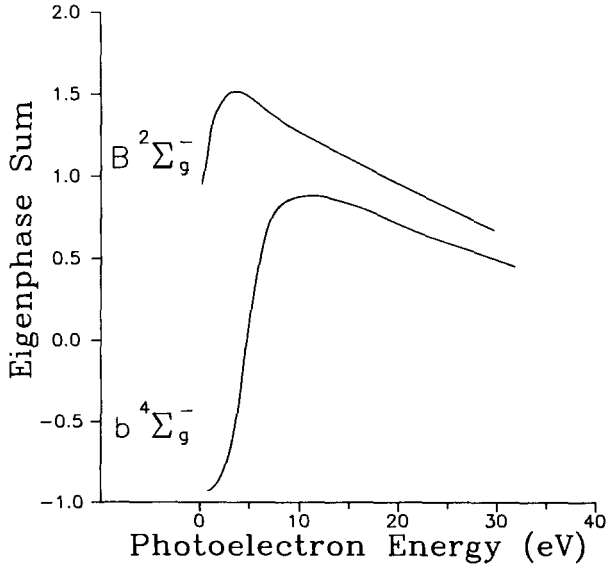

FIG. 1. Multiplet-specific eigenphase sums for the resonant $3\sigma_g \rightarrow k\sigma_u$ channel leading to the $b\,^4\Sigma_g^-$ ($3\sigma_g^{-1}$) and $B\,^2\Sigma_g^-$ ($3\sigma_g^{-1}$) ion states of O_2^+.

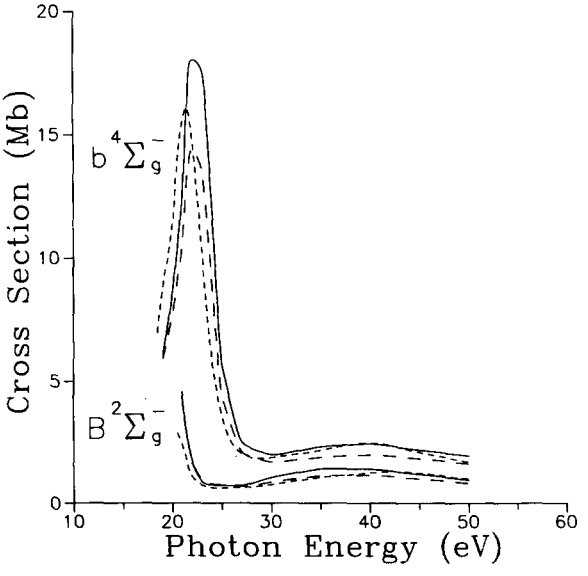

FIG. 3. Multiplet-specific cross sections for the $b\,^4\Sigma_g^-$ and $B\,^2\Sigma_g^-$ states of O_2^+:—and – –, present results in the dipole length and velocity forms, respectively; - - - Feshbach–Fano Stieltjes moment theory multiplet-specific results of Ref. 6.

each ion is due to the σ_u shape resonance seen in the associated eigenphase sums in Fig. 1. The weak maximum at higher energy in these cross sections arises from the energy dependence of the nonresonant $k\pi_u$ channel. These results show significant nonstatistical behavior near threshold, with the resonance maximum for the $b\,^4\Sigma_g^-$ state at a photoelectron energy of about 4 eV and the oscillator strength for the $B\,^2\Sigma_g^-$ cross section significantly shifted toward threshold. This behavior in the oscillator strength leads to a ratio of the quartet to doublet photoionization cross sections of over 15:1 just below 25 eV photon energy as shown in Fig. 4. These large deviations from statistical behavior are obviously not seen in studies with a multiplet-averaged potential which give a resonance position of ~ 3.5 eV above threshold for both ions.[7–10] At higher energies our results are in good agreement with these studies[7–10] and show the expected 2:1 statistical ratio.

In Fig. 5 we compare our calculated $b\,^4\Sigma_g^-$ and $B\,^2\Sigma_g^-$ cross sections with the experimental data of Gustaffson.[13] At low photoelectron energy, the experimental cross sections are dominated by an autoionizing window resonance at ~ 21 eV involving Rydberg states leading to the $c\,^4\Sigma_u^-$ ion (IP = 24.5 eV)[13] and the $k\sigma_u$ shape resonant background. Higher resolution work shows this autoionizing structure at low energy in more detail,[14,15] as well as additional structure in the $b\,^4\Sigma_g^-$ cross section arising from Rydberg levels leading to the $B\,^2\Sigma_g^-$ ion.[14] In fact, a window resonance appears at nearly the same energy as the peak of the shape resonance in our calculated $b\,^4\Sigma_g^-$ cross section[14] and in the region of rapid increase in our calculated $B\,^2\Sigma_g^-$ cross section.[14,15] Although this autoionizing structure hinders a simple "assignment" of the shape resonance feature in the two multiplet cross sections, these high resolution studies show relatively broad shape resonance features at significantly different photoelectron energies for the two ions. The high resolution

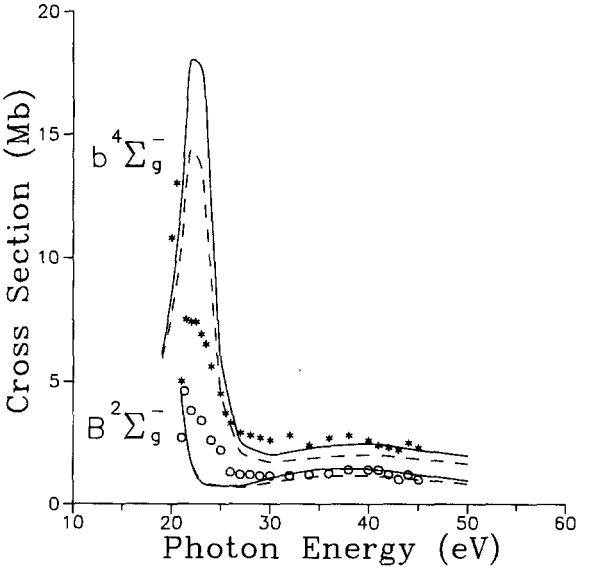

FIG. 5. Photoionization cross sections for the $b\,^4\Sigma_g^-$ and $B\,^2\Sigma_g^-$ states of O_2^+: — and – –, present results in the dipole length and velocity forms, respectively; *, experimental results of Ref. 13 for the $b\,^4\Sigma_g^-$ state; O, experimental results of Ref. 13 for the $B\,^2\Sigma_g^-$ state.

study of Morin *et al.*[14] shows a maximum in the cross section at 21.5 eV photon energy or about 3.5 eV kinetic energy for the $b\,^4\Sigma_g^-$ ion. The $B\,^2\Sigma_g^-$ cross section peaks at about 1 eV above threshold.[14,15] This can be seen more clearly in Fig. 6 which shows the $B\,^2\Sigma_g^-$ cross section on an expanded energy scale near threshold. Assignment of this maximum is hindered by the difficulty of obtaining accurate measurements at very low photoelectron energies.[15] Clearly, however, there is no shape resonant maximum in the $B\,^2\Sigma_g^-$ cross sections at 23 eV photon energy, as seen in previous theoretical studies using multiplet-averaged potentials.[7–10]

Figure 7 shows our calculated photoelectron asymme-

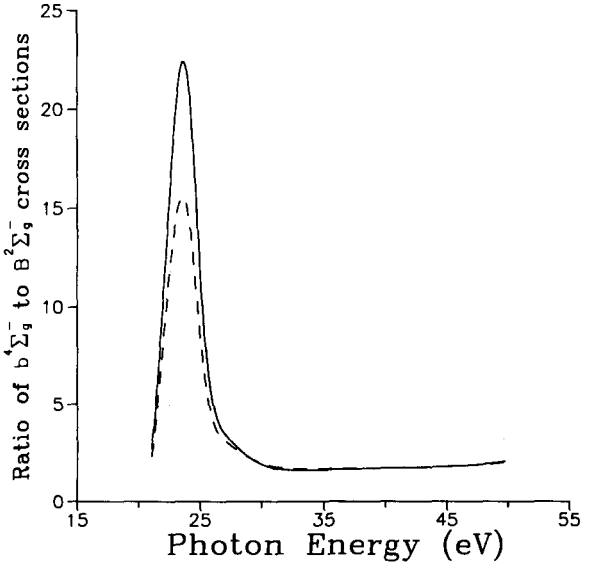

FIG. 4. Ratio of the calculated $b\,^4\Sigma_g^-$ cross section to the $B\,^2\Sigma_g^-$ cross section: — and – –, present results in the dipole length and velocity forms, respectively.

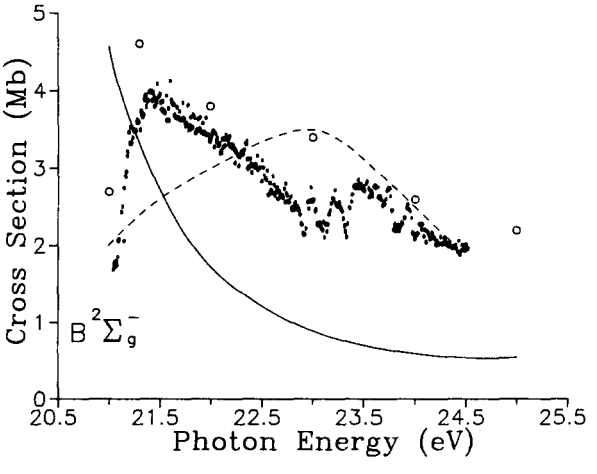

FIG. 6. Photoionization cross sections for the $B\,^2\Sigma_g^-$ state of O_2^+ near threshold: —, present results (length); - - -, calculated static-exchange vibrationally averaged results of Ref. 9 using a multiplet-averaged potential; O, experimental results of Ref. 13. The dots are the experimental total cross sections from Fig. 2 of Ref. 14. The structure at ~ 23 eV arises from autoionization as discussed in Refs. 14 and 15.

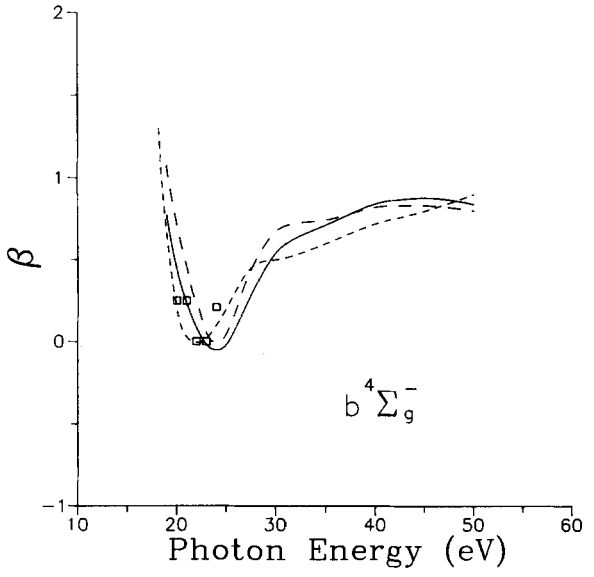

FIG. 7. Photoelectron asymmetry parameters for the $b\,^4\Sigma_g^-$ state of O_2^+: — and – –, present results in the dipole length and velocity forms, respectively; - - -, MSM calculations of Ref. 10 using a multiplet-averaged potential; □, experimental results of Ref. 21.

try parameters for the $b\,^4\Sigma_g^-$ state along with the data of Holmes *et al.*[21] and the multiple scattering model (MSM) calculations of Dittman *et al.*[10] using a multiplet-averaged potential. Both calculations are in good agreement with experiment and show a dip in the asymmetry parameter at roughly the resonance position of Fig. 3. In Fig. 8 we compare our calculated photoelectron asymmetry parameters for the $B\,^2\Sigma_g^-$ state with the results of MSM calculations of Dittman *et al.*[10] With the multiplet-averaged potential used in the MSM calculations the $B\,^2\Sigma_g^-$ asymmetry parameter is similar to that of the $b\,^4\Sigma_g^-$ state. The large differences between our results and the multiplet-averaged calculations of Dittman *et al.*[10] arise primarily from our use of a multiplet-specific potential and the resulting shift in the oscillator strength as discussed above. In Fig. 9 we show our calculated photoelectron asymmetry parameters for the $b\,^4\Sigma_g^-$ and $B\,^2\Sigma_g^-$ states to more clearly illustrate the large predicted multiplet-specific differences in β. Katsumata *et al.*[22] have reported values of 0.58 ± 0.06 and 1.05 ± 0.06 for β for the $b\,^4\Sigma_g^-$ ($v^+ = 0$) and $B\,^2\Sigma_g^-$ ($v^+ = 1$) ions respectively at the He I line (21.2 eV). Although these measurements cannot be directly compared to the present vibrationally unresolved results, they do show the same large qualitative differences between the quartet and doublet asymmetry parameters as seen in the present work. Continuum source measurements could provide considerable insight into the multiplet-specific behavior of these photoelectron angular distributions.

CONCLUSIONS

We have calculated photoionization cross sections and photoelectron angular distributions for the $3\sigma_g$ level of O_2 using Hartree–Fock photoelectron orbitals obtained with multiplet-specific potentials. These cross sections for the $b\,^4\Sigma_g^-$ and $B\,^2\Sigma_g^-$ ions show highly nonstatistical behavior arising from the sensitivity of the $k\sigma_u$ shape resonance to the exchange components of the different ion potentials seen by the photoelectron. Specifically, the oscillator strength associated with the σ_u shape resonance for the $B\,^2\Sigma_g^-$ ion is shifted to lower energy compared to that of the $b\,^4\Sigma_g^-$ cross section which peaks at ~ 4 eV above threshold. Our calculated cross sections agree well with the multiplet-specific Feshbach–Fano Stieltjes moment theory results of Winstead *et al.*[6] Previous theoretical studies using a multiplet-averaged potential could not distinguish such differences between the doublet and quartet photoelectron orbitals and

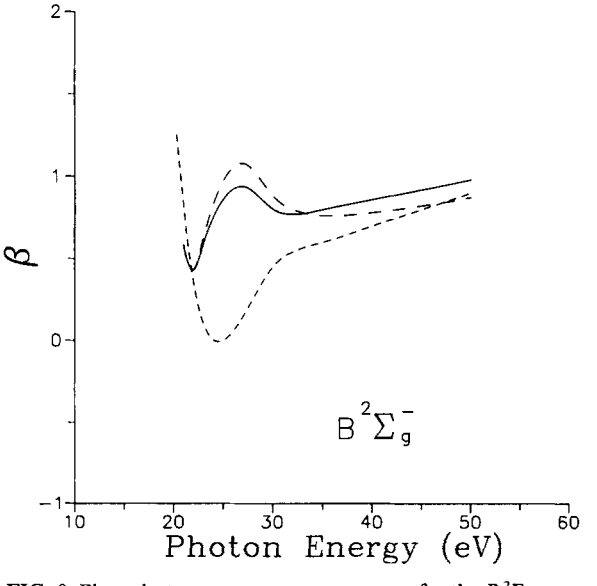

FIG. 8. Photoelectron asymmetry parameters for the $B\,^2\Sigma_g^-$ state of O_2^+: — and – –, present results in the dipole length and velocity forms, respectively; - - -, MSM calculations of Ref. 10 using a multiplet-averaged potential.

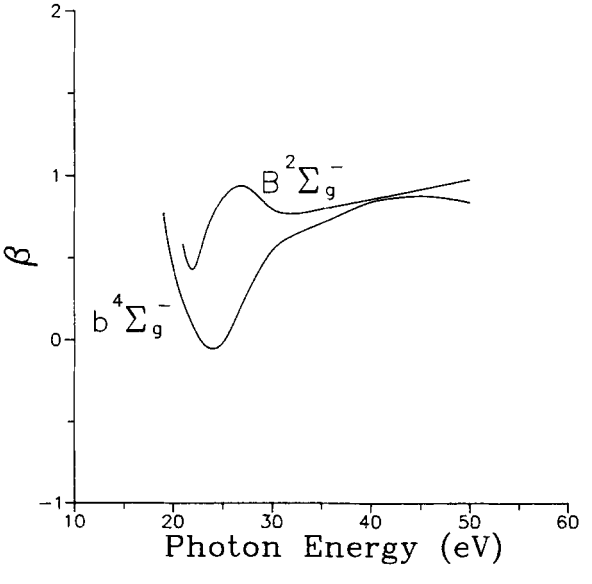

FIG. 9. Multiplet-specific photoelectron asymmetry parameters (length) for the $b\,^4\Sigma_g^-$ and $B\,^2\Sigma_g^-$ states of O_2^+.

hence led to a resonance peak at ~ 3.5 eV photoelectron kinetic energy for both ions.[7–10] Although autoionization structure complicates the photoelectron spectrum at low energy, high resolution experimental results do show that the σ_u shape resonance for the $B\,^2\Sigma_g^-$ ion appears much closer to threshold than that for the $b\,^4\Sigma_g^-$ ion.[14,15] These multiplet-specific effects are also seen in the photoelectron angular distributions where our results show substantial differences from the multiplet-averaged results of Dittman *et al.*[10] for the $B\,^2\Sigma_g^-$ ion in the shape resonance region. Continuum source measurements of the photoelectron angular distributions for the $B\,^2\Sigma_g^-$ ion would provide insight into such multiplet-specific effects. Above the shape resonance region our results agree well with previous calculations[7–10] as well as experimental results[11–13] and show the expected 2:1 statistical ratio.

ACKNOWLEDGMENTS

This work is supported by the National Science Foundation under Grant No. CHE8521391. The authors acknowledge use of the resources of the San Diego SuperComputer. The authors also thank Dr. C. L. Winstead for bringing the Feshbach–Fano Stieltjes moment theory results of his Ph.D. thesis to our attention.

[1]P. J. Miller and W. A. Chupka (private communication).
[2]J. A. Stephens, M. Braunstein, and V. McKoy (to be published).
[3]M. E. Smith, V. McKoy, and R. R. Lucchese, J. Chem. Phys. **82**, 4147 (1985).
[4]M. R. Hermann, C. W. Bauschlicher, Jr., W. M. Huo, S. R. Langhoff, and P. W. Langhoff, Chem. Phys. **109**, 1 (1986).
[5]P. M. Dehmer, J. L. Dehmer, and S. T. Pratt, Comments At. Mol. Phys. **19**, 205 (1987).
[6]C. L. Winstead *et al.* (to be published); see also C. L. Winstead, Ph.D. thesis, Indiana University, 1987.
[7]P. W. Langhoff, A. Gerwer, C. Asaro, and B. V. McKoy, Int. J. Quantum Chem. Symp. **13**, 645 (1979).
[8]A. Gerwer, C. Asaro, B. V. McKoy, and P. W. Langhoff, J. Chem. Phys. **72**, 713 (1980).
[9]G. Raseev, H. Lefebvre-Brion, H. Le Rouzo, and L. A. Roche, J. Chem. Phys. **74**, 6686 (1981).
[10]P. M. Dittman, D. Dill, and J. L. Dehmer, J. Chem. Phys. **76**, 5703 (1982).
[11]C. E. Brion, K. H. Tan, M. J. van der Wiel, and Ph. E. van der Leeuw, J. Electron Spectrosc. Relat. Phenom. **17**, 101 (1979).
[12]J. A. R. Samson, J. L. Gardner, and G. N. Haddad, J. Electron Spectrosc. Relat. Phenom. **12**, 281 (1977).
[13]T. Gustaffson, Chem. Phys. Lett. **75**, 505 (1980).
[14]P. Morin, I. Nenner, M. Y. Adams, M. J. Hubin-Franskin, J. Delwiche, H. Lefebvre-Brion, and A. Giusti-Suzor, Chem. Phys. Lett. **92**, 609 (1982).
[15]M. Ukai, A. Kimura, S. Arai, P. Lablanquie, K. Ito, and A. Yagishita, Chem. Phys. Lett. **135**, 51 (1987).
[16]R. R. Lucchese, K. Takatsuka, and V. McKoy, Phys. Rep. **131**, 147 (1986).
[17]R. R. Lucchese, G. Raseev, and V. McKoy, Phys. Rev. A **25**, 2572 (1982).
[18]T. H. Dunning and P. J. Hay, in *Modern Theoretical Chemistry*, edited by H. F. Schaefer III (Plenum, New York, 1976), Vol. 3, Chap. 1.
[19]W. J. Hunt and W. A. Goddard III, Chem. Phys. Lett. **3**, 414 (1969).
[20]U. Fano and J. W. Cooper, Rev. Mod. Phys. **40**, 441 (1968).
[21]R. M. Holmes and G. V. Marr, J. Phys. B **13**, 945 (1980).
[22]S. Katsumata, Y. Achiba, and K. Kimura, J. Electron Spectrosc. Relat. Phenom. **17**, 229 (1979).